

Figure S1. TF binding, mRNA expression, and DNA methylation in PGCs. **A** Heatmap of RPKM values within just binding sequences called by fimo, separated into those that have high DNase-signal in E16.5m PGCs (DNase-Hi, RPKM > 20) and those that have RPKM=0 (DNase-Lo). Rows are ordered by decreasing signal in of E14.5m. All stages shown are during PGC development. **B,C** Example region with DNase accessibility and low local DNA methylation throughout PGC development. CpG cov indicates the BS-seq read coverage. TF binding sequences called by fimo that overlap the peak summit in E14.5m are shown. **D** RNA-seq levels in the indicated stages of PGC development for TFs that are expressed in E16.5m PGCs and were significantly enriched in a motif analysis at E14.5m PGC DNase-Hi sites. (Related to Figure 1).

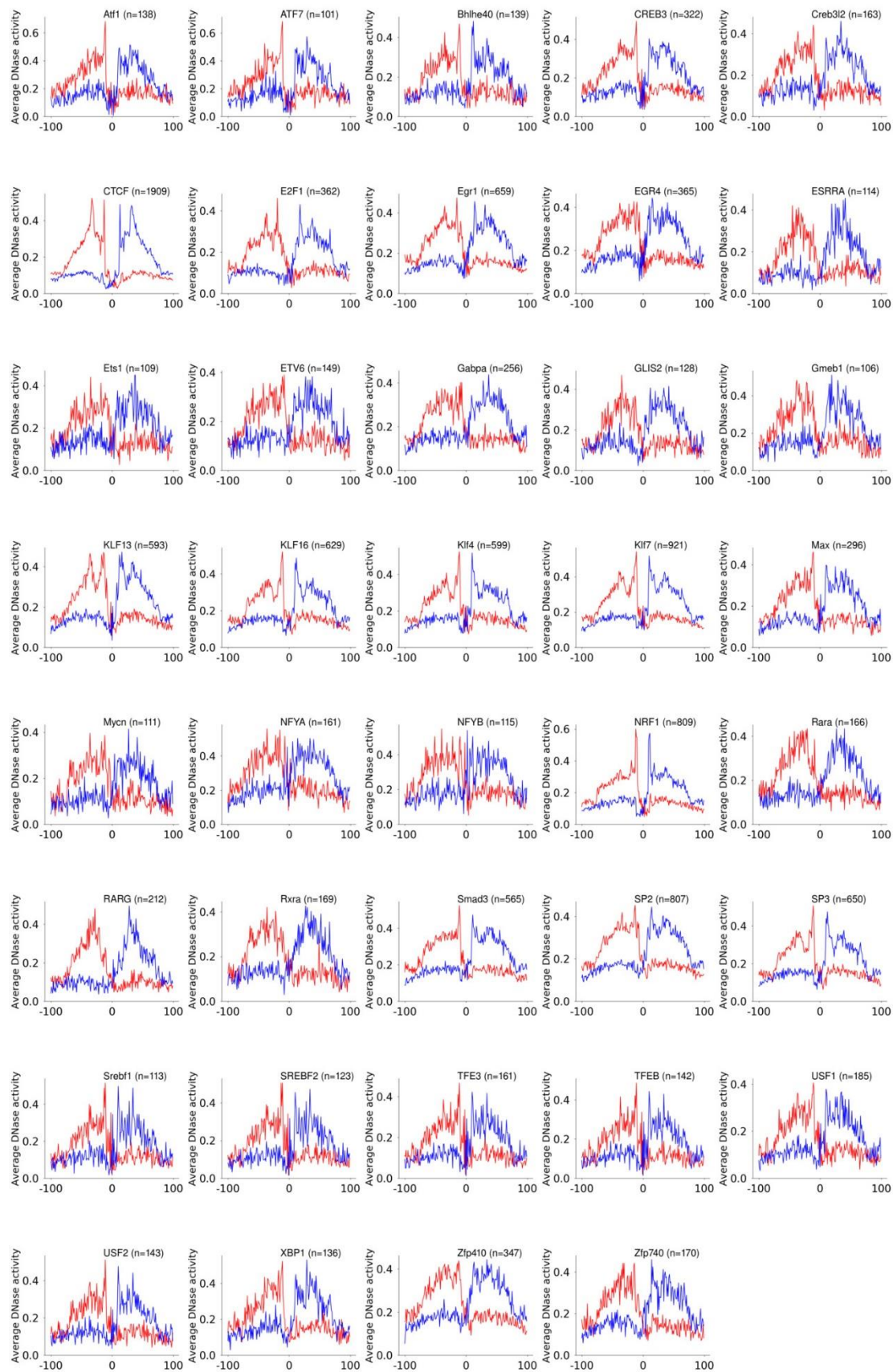


Figure S2. Average DNase-seq footprint profiles in E14.5m PGCs at E14.5m PGC DNase-Hi sites containing binding sequences for the indicated TFs (Related to Figure 1).

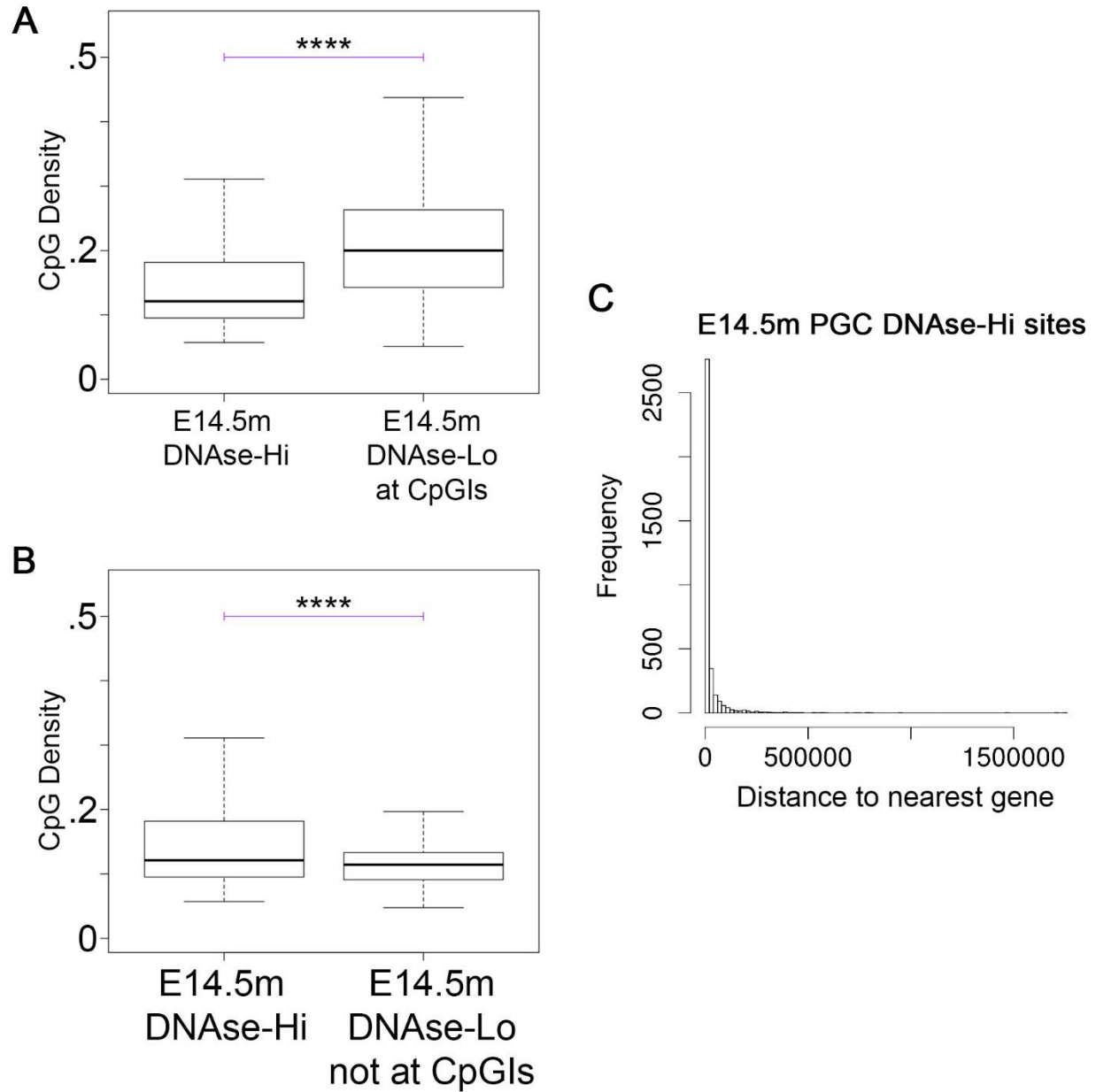


Figure S3. Additional Data on E14.5m PGC DNase-Hi Sites. A Boxplots comparing the distribution of CpG densities at E14.5m PGC DNase-Hi sites to the distribution at DNase-Lo sites within a CpG island (CpGI). B Boxplots comparing the distribution of CpG densities at E14.5m PGC DNase-Hi sites to the distribution at DNase-Lo sites not at a CpGI. P-vals in A and B were calculated by the Wilcoxon Test and are indicated as follows: * $P < .01$; ** $P < .001$; *** $P < 10^{-5}$; **** $P < 10^{-10}$. C Histogram of distances (in nucleotides) from E14.5m PGC DNase-Hi sites to the nearest gene. (Related to Figure 1).

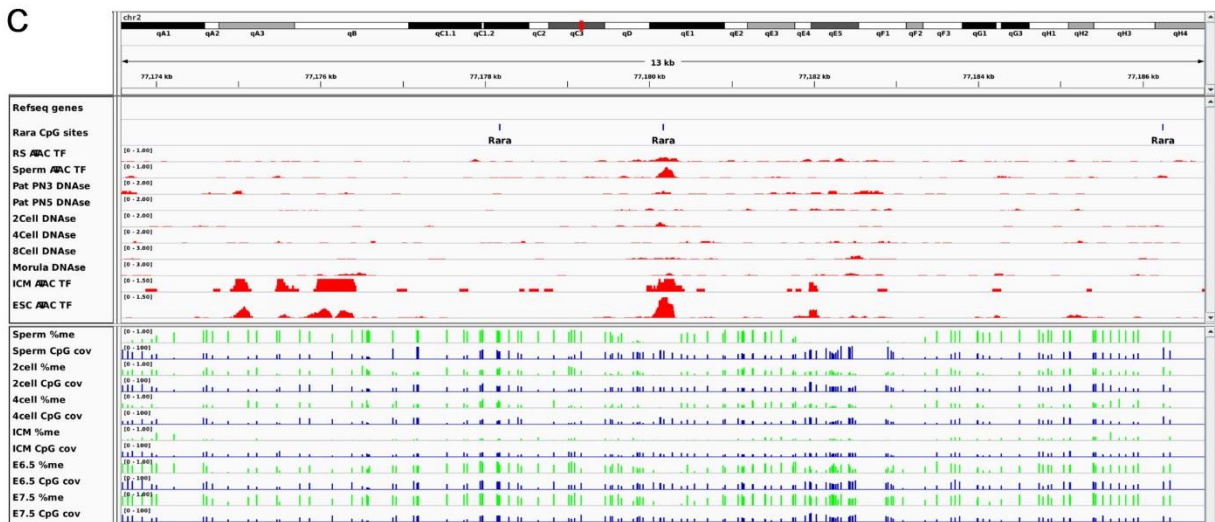
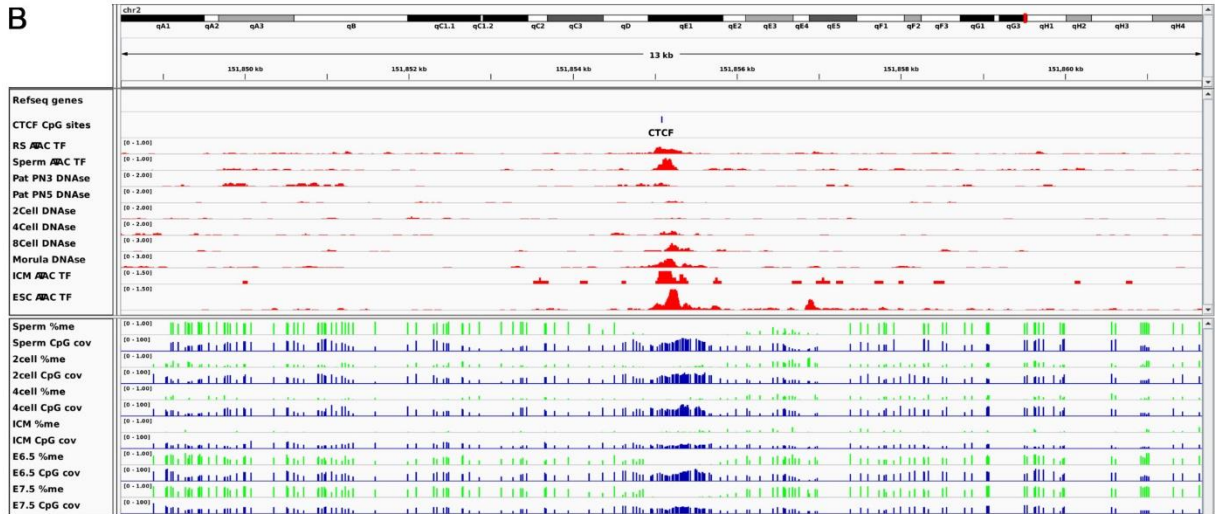
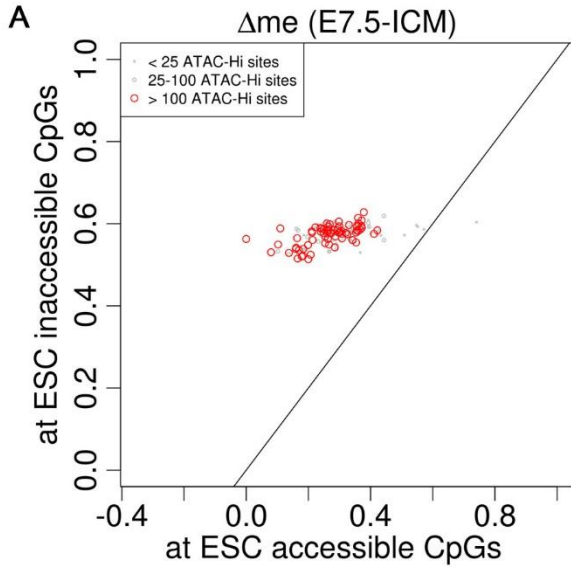


Figure S4. TF binding and DNA methylation of sperm and pre-implantation embryos at E14.5m PGC DNase-Hi and -Lo sites. **A** Scatterplot of changes in DNA methylation between E14.5m and E16.5m PGCs. Each point represents the average methylation change (fraction meCpG in E16.5m minus E13.5m PGCs) at CpGs overlapping a binding sequence for a specific TF. The x-axis gives the average value for E14.5m PGC DNase-Hi sites, while the y-axis gives the average value for DNase-Lo sites. **B,C** Example regions showing TF accessibility and DNA methylation in preimplantation embryos at E14.5m PGC DNase-Hi sites. CpG cov indicates the BS-seq read coverage. TF binding sequences called by fimo that overlap the peak summit in E14.5m are shown. (Related to Figure 2).

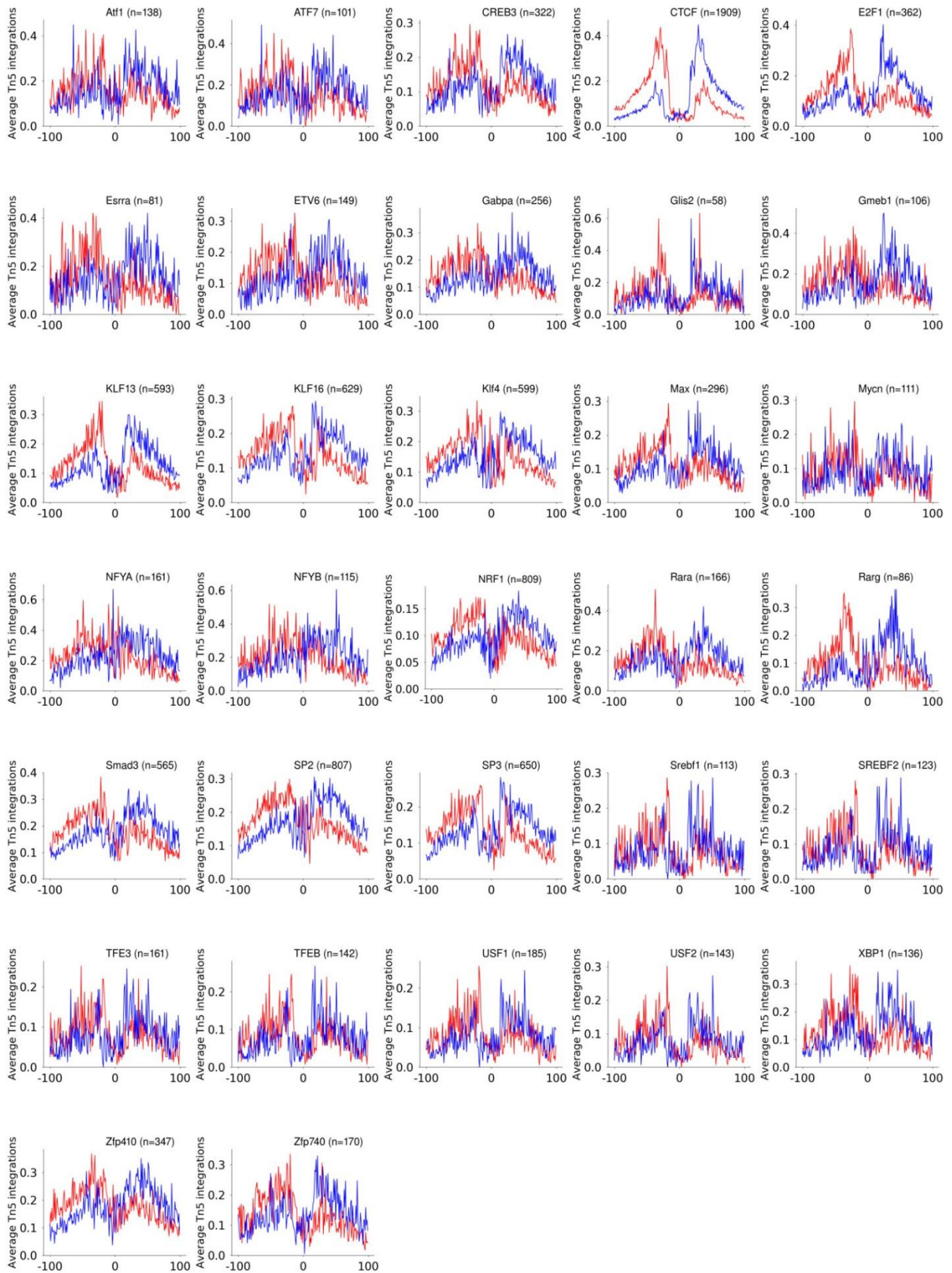


Figure S5. Average ATAC-seq footprint profiles in ESCs at E14.5m PGC DNase-Hi sites containing binding sequences for the indicated TFs. (Related to Figure 2).

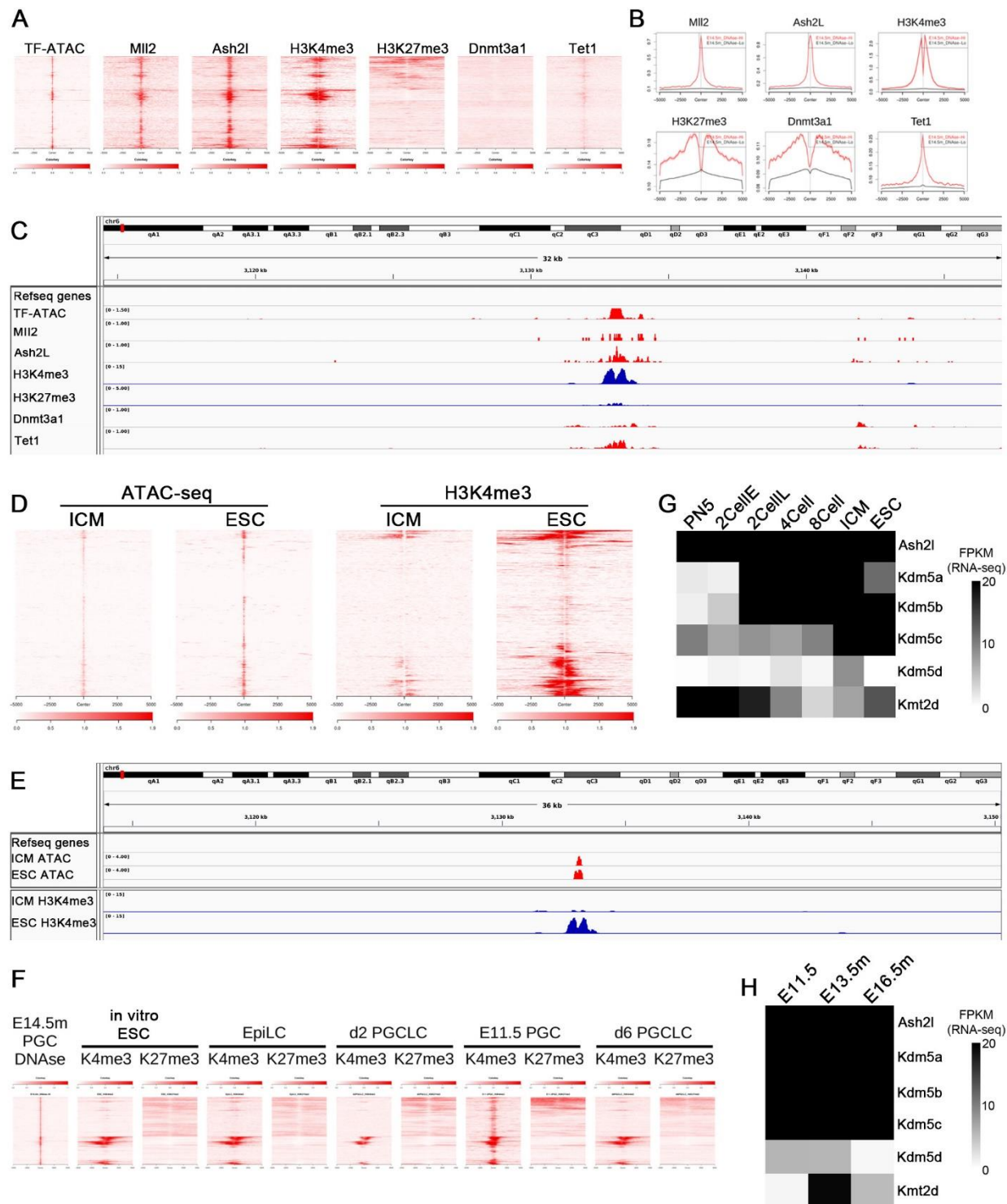


Figure S6. Co-factors at E14.5m PGC DNase-Hi sites. **A** Heatmaps of the given ChIP-seq signal type in ESCs, centered at E14.5m PGCDNase-Hi sites. TF-ATAC signal in ESC's is also shown for comparison. **B** Average profile of the given signal in ESCs at E14.5m PGC DNase-Hi vs DNase-Lo sites. **C** An example of an E14.5m PGC DNase-Hi site, showing enrichment for the data used in A and B. **D** Heatmaps showing enrichment of TF-ATAC and H3K4me3 ChIP-

seq in ICMs vs. ESCs at E14.5m PGC DNase-Hi sites. **E** An example showing ICM and ESC H3K4me3 ChIP-seq and TF-ATAC signal at an E14.5m PGC DNase-Hi site. **F** Heatmaps showing H3K4me3 and H3K27me3 signal at E14.5m PGC DNase-Hi sites for epiblast-like cells (EpiLCs), PGC-like cells 2 days and 4 days after induction (d2 PGCLCs and d4 PGCLCs, respectively), and E11.5 PGCs. The EpiLCs and PGCLCs were derived from the in vitro ESCs. **G,H** RNA-seq expression heatmap of the indicated histone demethylases and methyltransferases (G) in pre-implantation embryos and (H) PGCs. (Related to Figure 2).

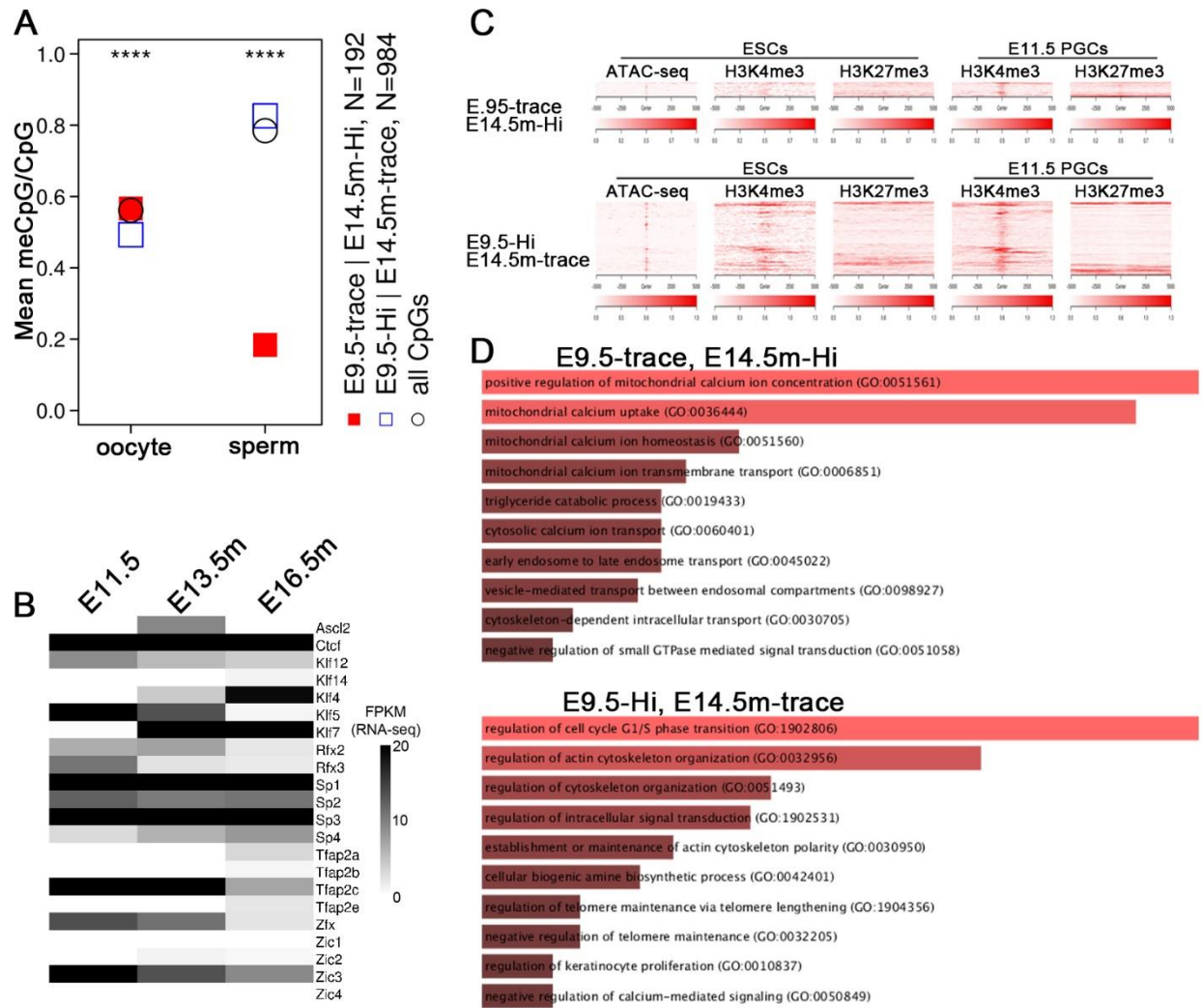


Figure S7. DNA methylation, co-factor binding, and mRNA expression at E9.5-trace, E14.5m-Hi and E9.5-Hi, E14.5m-trace sites. **A** Average DNA methylation levels as in Figure 3B, comparing sperm to oocyte methylation. P-values are by Fisher's exact test. P-val cutoffs (E9.5-trace, E14.5m-Hi vs E9.5-Hi, E14.5m-trace) * $P < 0.01$; ** $P < 10^{-3}$; *** $P < 10^{-5}$; **** $P < 10^{-10}$. **B** RNA-seq of TFs enriched at E9.5-Hi, E14.5m-trace sites (Figure 3H). **C** Heatmap showing TF-ATAC in ESCs along with H3K4me3 and H3K27me3 ChIP-seq in ESCs and E11.5 PGCs, sorted by hierarchical clustering. **D** Relative Enrichr score of significantly enriched "GO Biological Process" terms for genes within 10 kb of the indicated set of loci. Only genes with FPKM > 10 in E16.5m were considered for the E9.5-trace, E14.5m-Hi set, whereas only genes with FPKM > 10 in E11.5 were considered for the E9.5-Hi, E14.5m-trace set. All pathways shown have $P < .05$. (Related to Figure 3).

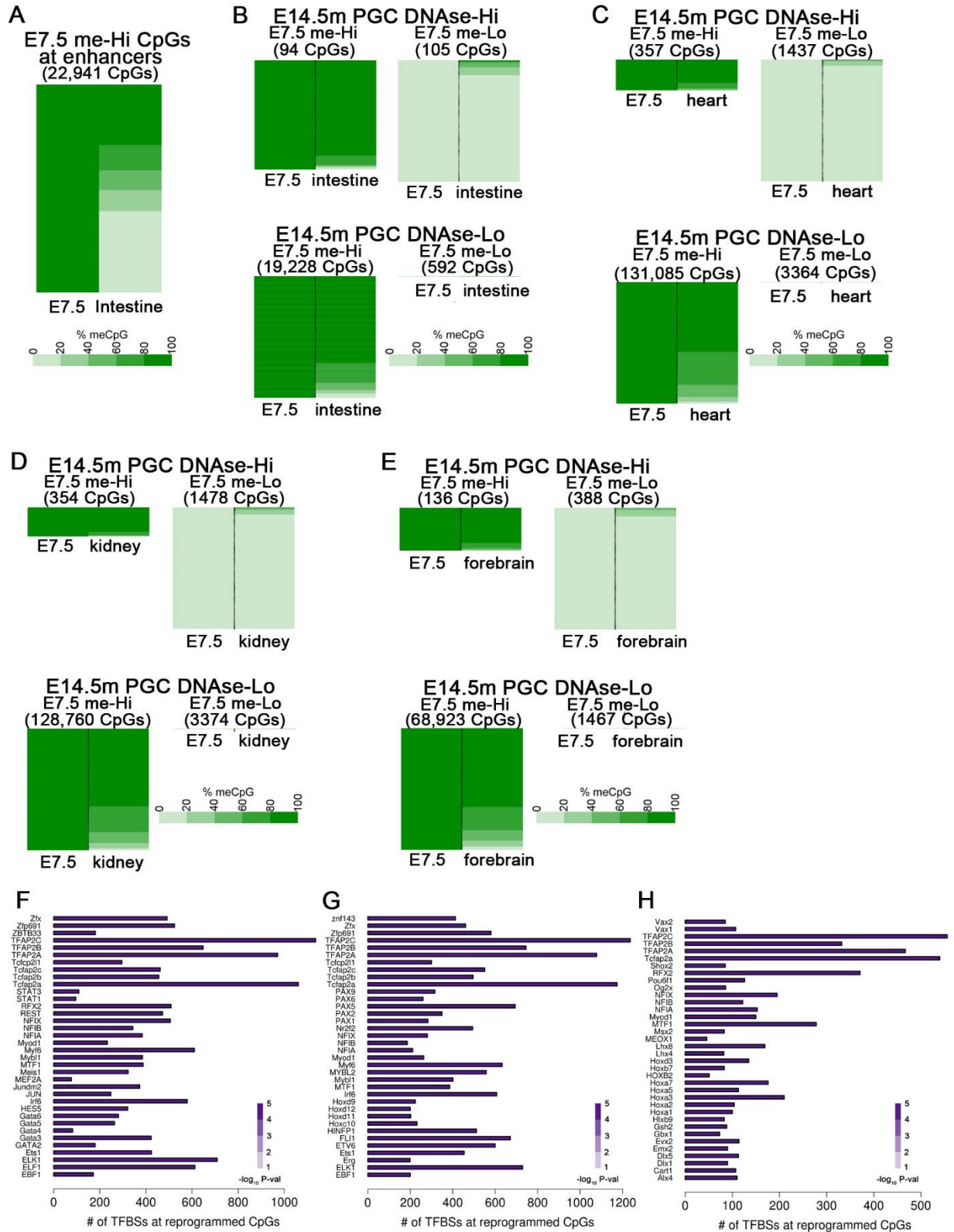


Figure S8. DNA methylation maintenance from E7.5 embryos to neonatal and adult tissues. **A** Heatmap of CpG methylation percentage for all CpGs with > 80% methylation in E7.5 embryos that overlap with a published ATAC-seq peak in either embryonic, fetal, or adult intestine. The legend in A also applies to panels B-E. **B** Heatmap as described in Figure 4A, except that here only CpGs that do not overlap a published ATAC-seq peak from fetal, embryonic, or adult intestinal tissue are considered. **C-E** Heatmaps as in Figure 4A, except that instead of adult intestine, methylation is examined from BS-seq of neonatal heart (C), kidney (D), and forebrain (E). **F-H** Bar plots showing the number of motifs and the statistical significance of motif enrichment for the indicated TFs at CpGs with > 80% methylation in E7.5 embryos and < 20% methylation in neonatal heart (F), kidney (G), and forebrain (H). (Related to Figure 4).

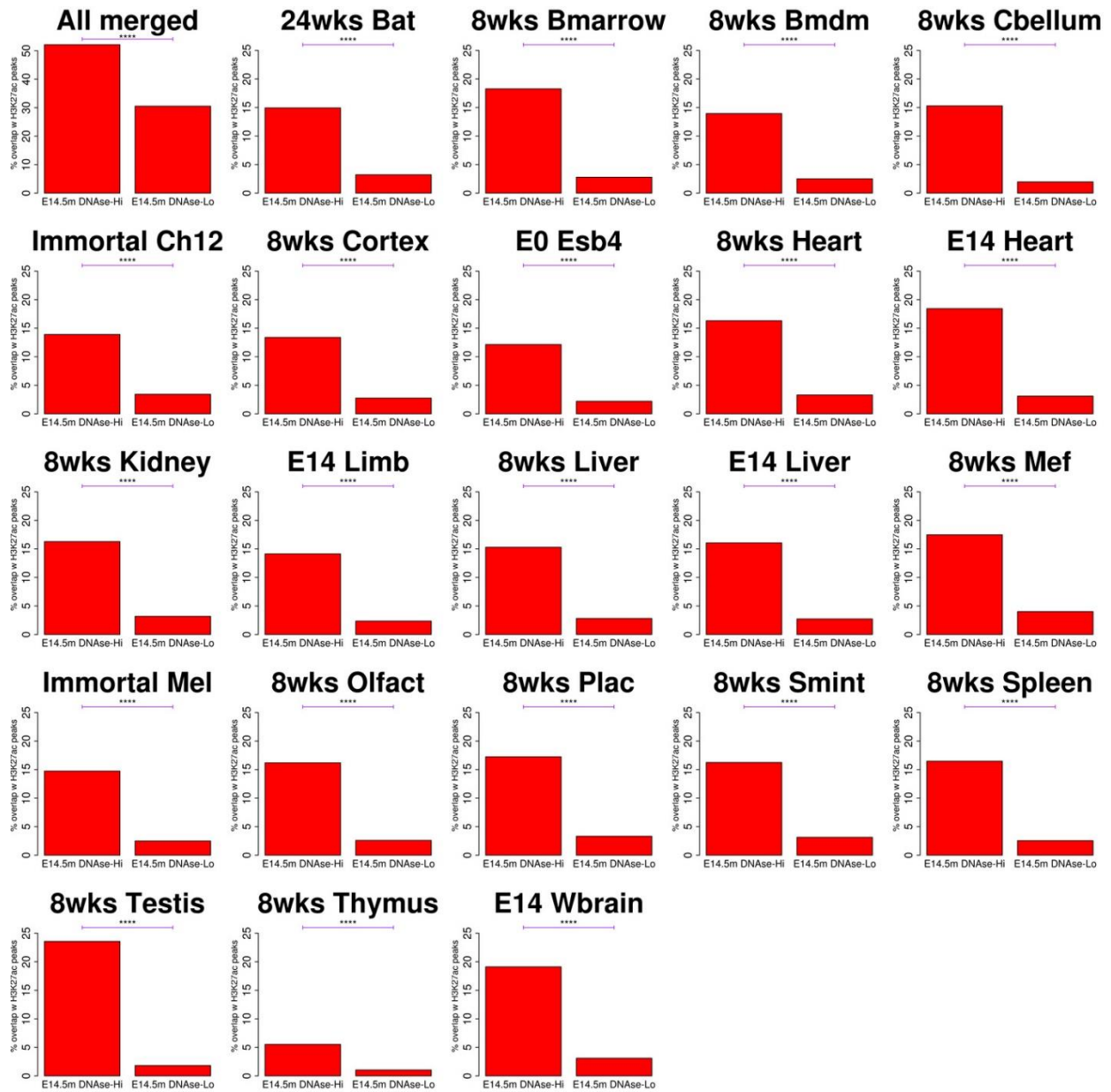
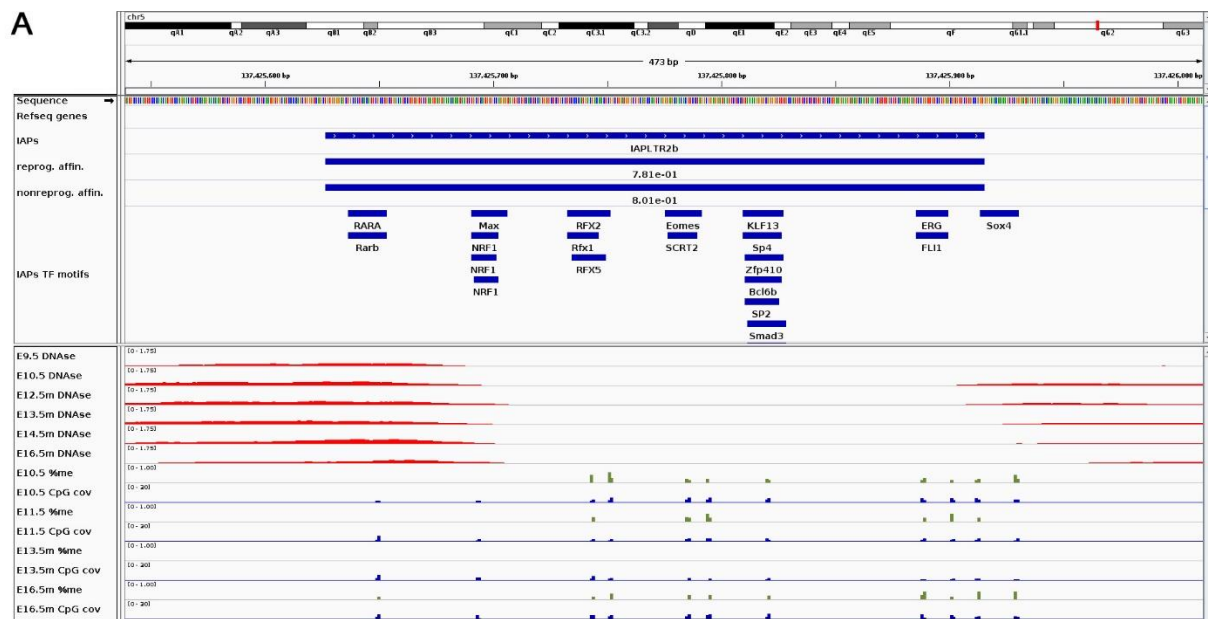


Figure S9. Overlap of E14.5m PGC DNase-Hi and DNase-Lo sites with H3K27ac peaks from the indicated tissue. “All merged” shows the overlap with all peaks from all samples combined. P values were determined by Fisher’s exact test, and cutoffs are as follows: * $P < .01$; ** $P < .001$; *** $P < 10^{-5}$; **** $P < 10^{-10}$. (Related to Figure 4).

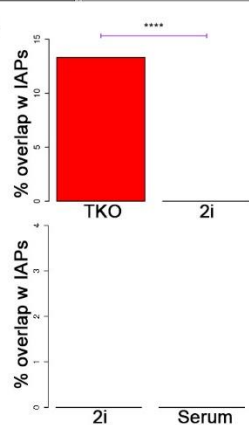
A



B



C



D

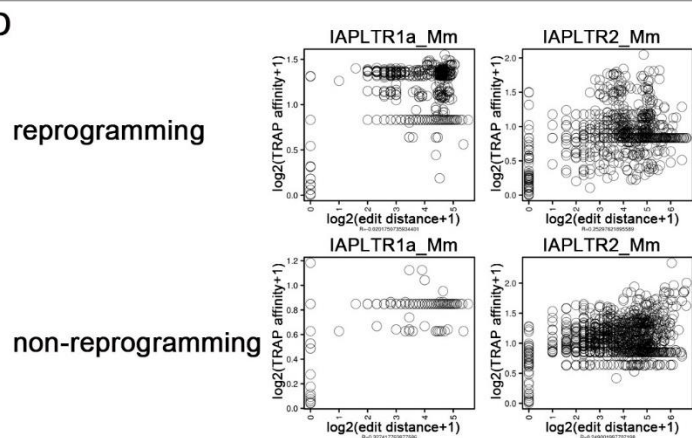


Figure S10. TF binding and sequence content at IAPs. **A,B** Examples showing DNase-seq and DNA methylation levels during PGC development at IAP LTRs that have evidence of TF binding. Tracks showing the highest TRAP affinity of the E16.5m PGC putative reprogramming TFs, and of E16.5m PGC non-reprogramming TFs, at the whole IAP, are displayed under the IAP track. **C** The proportion of Nrf1 peaks overlapping with IAPs in ESC with Dnmt triple knockout (TKO), in 2i medium, and in serum. . P-vals were calculated by Fisher's Exact Test and are indicated as follows: * $P < .01$; ** $P < .001$; *** $P < 10^{-5}$; **** $P < 10^{-10}$. **D** Scatterplots comparing TRAP affinities at IAPs to the edit distance to the consensus for IAPs of type IAPLTR1a_Mm and IAPLTR2_Mm, for putative reprogramming TFs and non-reprogramming re-methylation phase TFs, separately. Pearson's correlation coefficients are shown underneath each scatterplot. (Related to Figure 6).

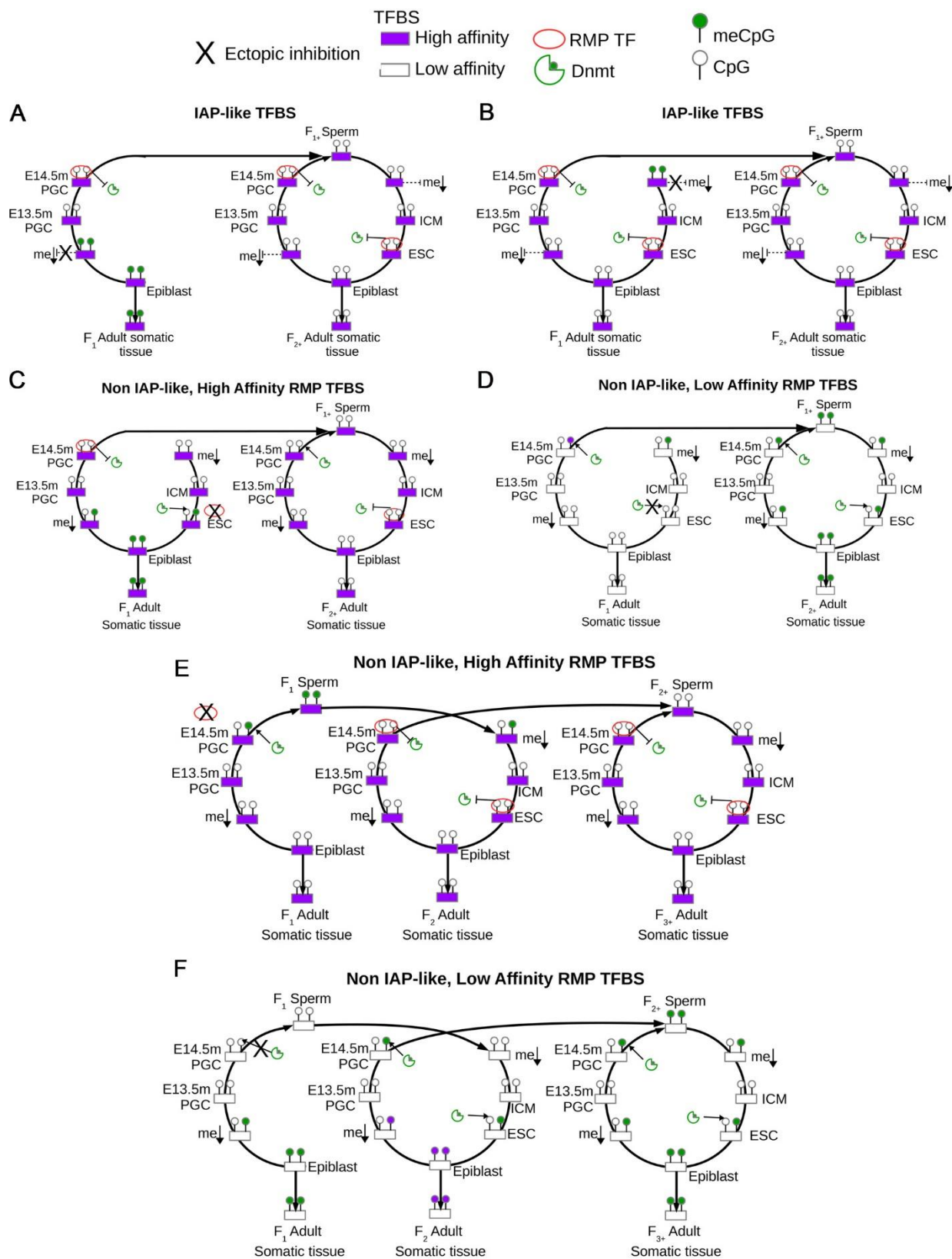


Figure S11. Predicted mechanisms of trans-generational and inter-generational epigenetic inheritance. **A,B** The model predicts that trans-generational epigenetic inheritance would occur by ectopically inhibiting de-methylation resistance at IAP-like loci either during PGC development (A) or during pre-implantation development (B). These sites are normally methylated throughout the entire cycle (Figure 7C). Inhibition at either stage would result in trans-generational epigenetic inheritance at sites with a high affinity for re-methylation phase (RMP) TFs. However, inhibiting de-methylation resistance in PGCs would result in the induced phenotype being skipped in adult somatic tissue of the F₁ offspring (A), whereas inhibiting it during pre-implantation development would result in the phenotype being present in the F₁ adult somatic tissues (B). Inhibition of de-methylation resistance might result from ectopic over-expression of a reprogramming TF such as Esrra, and possibly from ectopic changes in ncRNA expression. **C-F** The model predicts that inter-generational epigenetic inheritance would occur by ectopically inhibiting re-methylation or the abundance of RMP TFs at either low or high affinity RMP TFBSs, either during the PGC RMP or the post-ICM RMP. Such inhibition could be induced by changes in ncRNA expression, histone modifications, or direct changes in RMP TF expression. Other mechanisms of inter-generational epigenetic inheritance that are independent of DNA methylation are possible wherein ncRNA from sperm are passed to the pre-implantation embryo, but this mode is not shown as we are focused on the mechanistic consequences of our model. (C) Inhibiting a RMP TF in the post-ICM RMP would result in hypermethylation in the F₁ adult somatic tissue whereas these loci are normally hypomethylated in adult somatic tissue (Figure 7B). The F₁ sperm would be hypomethylated as usual because in the RMP of PGCs, TF binding at this locus would be restored. All subsequent generations would revert back to the normal behavior. (D) Inhibiting post-ICM re-methylation at a low affinity RMP TFBS would result in that site being hypomethylated in F₁ adult somatic tissue whereas these loci are typically hypermethylated in adult somatic tissue (Figure 7A). F₁ sperm would revert back to being hypermethylated because re-methylation is restored to normal levels in PGCs, and all subsequent generations would have a normal phenotype. (E) Inhibiting a RMP TF binding to a high-affinity site during the PGC RMP would result in hypermethylation in the F₁ sperm whereas these loci are typically hypomethylated in sperm. The phenotype of the pre-implantation embryo would be affected, but normal binding of the TF in the post-ICM RMP would restore hypomethylation to this site in all subsequent adult somatic tissues and sperm. (F) Inhibiting re-methylation at a low-affinity RMP TFBS in the PGC RMP would result in hypomethylation of the F₁ sperm whereas these sites are typically hypermethylated in sperm (Figure 7A). The phenotype of the pre-implantation embryo would be affected, but subsequently, all adult somatic tissues and sperm will be restored to the normal phenotype because of normal re-methylation in the RMPs. (Related to Figure 7).